Journal of Functional Materials and Applied Engineering

Research Paper

Photothermal and Antibacterial Properties of Ti-Nb-Zr-Ta Medium Entropy Alloy Thin Films

Teddy Gupta[1], Anuj Fossel[2], Deepa Roman[2,*]

[1] Chemistry Department, University of Waikato, Private Bag 3105, Hamilton, New Zealand
[2] Department of Production Engineering, Warsaw University of Life Sciences, 02-776 Warsaw, Poland
*Corresponding author: deeparoman@gmail.com

Abstract. This investigation seeks to elucidate the photothermal conversion characteristics and antimicrobial efficacy of Ti-Nb-Zr-Ta medium entropy alloy coatings with compositionally and microstructurally varied architectures. A suite of Ti-Nb-Zr-Ta MEA coatings was fabricated via magnetron sputtering at oblique incidence angles of 0°, 45°, and 80°. The composition, elemental valence states, phase constitution, and morphology of the films were characterized. Optical absorption and photothermal conversion capabilities were tested, and the biocompatibility and antibacterial properties were evaluated. Results The crystal structure of the Ti-Nb-Zr-Ta MEA films was identified as body-centered cubic (BCC). As the incident angle increased, the content of Ti and Nb increased, while Zr and Ta decreased; oxygen content increased, columnar tilting angles increased, structures became looser, and surface roughness increased. Due to the multiple reflection absorption of light by loose columnar crystals and enhanced plasmon resonance resulting from the porous structure, the optical absorption and photothermal temperature rise of the films improved. Under infrared irradiation, the film temperature rose rapidly; the film deposited at 80° reached a maximum temperature of 110°C after 3 minutes of 808 nm irradiation (2 W/cm²). The films exhibited overall antibacterial capability, completely eradicating adherent colonies after 10 minutes of infrared irradiation on the 80° film. The films also demonstrated excellent biocompatibility, allowing fibroblasts to proliferate naturally on their surfaces. Conclusion Ti-Nb-Zr-Ta MEA thin films deposited by oblique-angle magnetron sputtering exhibit enhanced photothermal properties due to the "light trap" structure formed by loose columnar crystals, endowing the films with photothermal antibacterial capabilities.

Keywords: *Magnetron sputtering; Oblique incidence; Ti-Nb-Zr-Ta; Medium entropy alloy; Photothermal properties; Antibacterial properties*

Received on 15 Dec 2021, Accepted on 15 Apr 2022, Published on 28 Apr 2022

1 Introduction

Titanium, niobium, zirconium, and tantalum, both in elemental and alloyed forms, represent a distinguished category of metallic biomaterials celebrated for their outstanding tissue compatibility [1], elastic stiffness approximating human cortical bone [2], and propensity to develop compact, passivating oxide surface layers (principally TiO_2, Nb_2O_5, ZrO_2, and Ta_2O_5) [3]. These oxide layers significantly enhance the corrosion resistance of implants in physiological environments, inhibit the release of potentially toxic metal ions, and minimize inflammatory or immune responses [3]. Furthermore, these elements exhibit good processability, making them amenable to various manufacturing techniques [4]. Accordingly, Ti-Nb-Zr-Ta alloy systems have attracted considerable research interest for fabrication of orthopedic and cardiovascular medical devices, including osseointegration screws, arthroplasty components, endovascular stents, and dental endosseous implants [5].

Recent research has focused on optimizing the properties of these quaternary alloys. Xiang et al. [6] successfully prepared Ti-Nb-Zr-Ta medium entropy alloys (MEAs) with high strength and good biocompatibility by precisely adjusting the atomic ratios of the constituent elements. Li et al. [7] reported that Ti-Nb-Zr-Ta alloys exhibit excellent wear resistance, a critical factor for load-bearing implants. Mustafi et al. [8] highlighted that these alloys

are stronger and lighter than pure tantalum, with surfaces capable of forming continuous Ta_2O_5 films that offer superior corrosion resistance. Guo et al. [9] established that Ti-Ta-Nb-Zr alloy porous constructs substantially surpassed conventional Ti6Al4V scaffolds in enhancing human bone marrow-derived mesenchymal stem cell proliferation, osteogenic commitment, and phenotypic maturation under in vitro conditions. In vivo investigations further corroborated that Ti-Ta-Nb-Zr architectures more potently stimulated de novo bone formation and implant-host osseointegration relative to Ti6Al4V equivalents. Achache et al. [10] employed magnetron sputtering to deposit Ti-Nb-Zr-Ta alloy films and systematically investigated the influence of deposition parameters, finding that under optimized conditions, the films possessed a low Young's modulus and high elastic deformability. Collectively, these studies underscore the immense potential of Ti-Nb-Zr-Ta alloys and their thin films in the manufacturing and surface modification of implantable medical devices.

However, a persistent clinical challenge associated with implanted medical devices is the risk of infection, which often necessitates prolonged courses of antibiotics [11]. Clinical treatments for such infections face significant hurdles, including the protective nature of biofilms and the rising tide of bacterial resistance [12]. While the release of antimicrobial metal ions (e.g., Ag^+, Cu^{2+}, Zn^{2+}) from the implant surface represents an emerging strategy for combating infection [13], it is often accompanied by concerns regarding uncontrollable release kinetics, potential cytotoxicity from metal ion accumulation, and the risk of compromising the mechanical integrity of the implant due to corrosion [14].

Photothermal therapeutic intervention has evolved into a compelling non-antibiotic strategy for microbial infection control. This technique involves the introduction of photothermal conversion materials that, upon irradiation with near-infrared (NIR) light, convert light energy into localized heat, elevating the temperature at the infection site to lethal levels for bacteria [15]. Compared to metal ion release strategies, photothermal antibacterial action avoids the risks associated with uncontrolled ion release and offers the advantages of spatiotemporal controllability and high local efficacy. Conventional photothermal transduction agents encompass noble metal nanostructures (e.g., Au, Ag), carbonaceous nanomaterials (e.g., graphene, carbon quantum dots), transition metal chalcogenides and oxides, and electrically conductive polymers (e.g., polypyrrole, polydopamine) [16].

High-entropy and medium-entropy alloys, distinguished by their multi-principal-element configurations, exhibit intrinsically wide energy band distributions arising from electronic state hybridization. This feature allows them to exhibit high optical absorption across ultraviolet, visible, and near-infrared bands, endowing them with superior photothermal conversion capabilities compared to noble metals or polymers [17, 18]. Moreover, the excellent thermal stability and biocompatibility of these alloys make them safer and more durable for photothermal applications. While introducing elements like Ag or Cu can further tailor properties, it may inadvertently compromise the thermodynamic stability and corrosion resistance of the alloy system [19]. An alternative and highly effective strategy to enhance photothermal performance without sacrificing stability is to engineer micro/nanostructures (e.g., protrusions, grooves, pores) on the material's surface. Such architectures increase the optical path length, trap light via multiple reflections, and enhance localized electromagnetic fields, thereby boosting light absorption and photothermal conversion efficiency [20].

Conventional methods for creating these surface architectures, such as templating, etching, and laser processing, typically involve complex, multi-step procedures and increase fabrication costs [21]. Within the domain of magnetron sputtering for coating fabrication, oblique-angle deposition—alternatively termed glancing angle deposition—has evolved into an innovative, photolithography-free methodology for producing micro- and nanostructured coatings. Throughout this process, source material is ejected from the target and condenses onto the substrate surface at a tilted incidence relative to the surface normal. The inherent "shadowing effect" causes adatoms to preferentially deposit on the tops of existing surface features, leaving the sides and shadowed regions less populated. This self-organized growth process leads to the formation of tilted, porous columnar structures (e.g., nanorods, helices) [22]. By adjusting the incident angle and substrate rotation, the morphology and orientation of these structures can be precisely controlled, offering a powerful tool for manipulating the optical and thermal properties of the film.

Therefore, this study employs oblique-angle magnetron sputtering to deposit Ti-Nb-Zr-Ta MEA thin films on Si and 316L stainless steel substrates. By systematically varying the substrate angle relative to the target, we aim

to modulate the film's composition, microstructure, and morphology. We investigate the relationship between the deposition geometry, the resulting film structure, and the optical absorption, photothermal conversion efficiency, biocompatibility, and antibacterial performance of the Ti-Nb-Zr-Ta MEA films.

2. Experimental Section

2.1 Materials and Substrate Preparation

Single-crystal silicon wafers (10 mm × 10 mm) and 316L stainless steel discs (ϕ10 mm × 2 mm, mirror-polished) were used as substrates. Substrate pretreatment involved sequential sonication in acetone and absolute ethanol (10 min each), followed by high-purity nitrogen stream desiccation prior to coating deposition. A mosaic target (Fig. 1a) was fabricated by assembling high-purity (99.9%) rectangular strips (3 mm × 135 mm × 3 mm) of Ti, Nb, Zr, and Ta in specific proportions to achieve a nominal equiatomic composition.

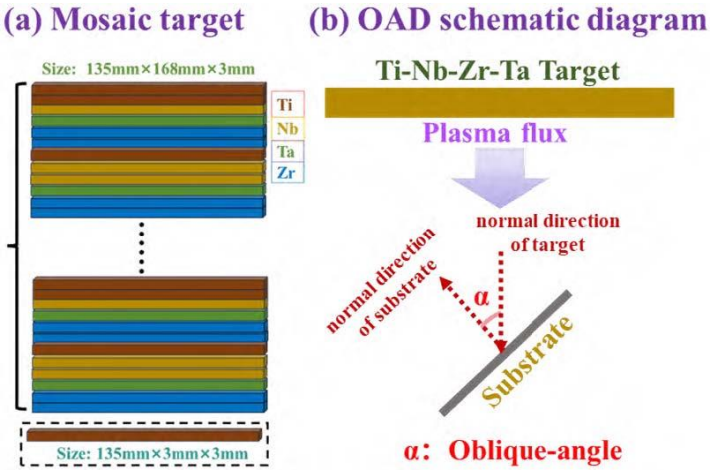

Figure 1 Mosaic-assembled Ti-Nb-Zr-Ta sputtering target (a); schematic of oblique-angle (glancing-angle) deposition (b)

2.2 Thin Film Deposition

Ti-Nb-Zr-Ta MEA coatings were fabricated via direct current magnetron sputtering. Chamber base pressure was maintained at ≤ 2×10^{-3} Pa prior to deposition. Ultra-high purity argon (99.999%) was introduced to establish 0.4 Pa working pressure for target pre-conditioning (250 V, 2 A, 10 min) to eliminate surface oxide contamination. Subsequently, the substrates were subjected to plasma etching (pulse bias 1000 V, pulse current 0.2 A) at 3.0 Pa for 15 minutes to eliminate any adsorbed contaminants. The Ti-Nb-Zr-Ta films were then deposited at a target power density of 2.2 W/cm², a working pressure of 0.6 Pa, and a duration of 20 minutes without intentional substrate heating. The influence of deposition geometry was examined by varying the inclination angle α between substrate surface normal and target surface normal to 0°, 45°, and 80° (Fig. 1b). The target-to-substrate distance was fixed at 80 mm, and the substrates were kept stationary during deposition to maximize the shadowing effect.

2.3 Characterization and Performance Testing

Film stoichiometry was determined via Energy Dispersive Spectroscopy. Surface and cross-sectional architecture, together with topographical roughness, were characterized by Scanning Electron Microscopy (Thermo Scientific) and Atomic Force Microscopy (Bruker). Crystallographic phase identification was performed through X-Ray Diffraction (Rigaku) using Cu Kα excitation. Electronic structure and chemical speciation were probed by X-Ray Photoelectron Spectroscopy (Thermo Fisher). Optical absorbance across the 200–1200 nm spectral range was quantified using a UV-Vis spectrophotometer (Shimadzu). Photothermal properties were evaluated using an 808 nm diode laser and an FLIR-E4XT infrared thermal camera, recording temperature changes every 30 seconds. The photothermal conversion efficiency was calculated based on the temperature rise curves. Antibacterial

performance against Escherichia coli(ATCC 25922) was assessed by counting colony-forming units (CFUs) after NIR irradiation. Biocompatibility was evaluated using mouse fibroblast cells (L929 or 3T3) via the CCK-8 assay to determine cell viability.

3. Results and Discussion

3.1 Chemical Composition and Valence State Analysis

EDS analysis revealed that the atomic ratios of the constituent elements varied significantly with the incident angle. For the film deposited at 0°, the Ti:Nb:Zr:Ta ratio was approximately 21:24:27:28. At 45°, this shifted to 24:25:25:26, and at 80°, it became 27:30:23:20. This phenomenon can be attributed to the scattering of sputtered atoms by the working gas (Ar). Lighter elements with smaller atomic radii, such as Ti and Nb, are more susceptible to scattering and angular deflection, allowing them to reach the substrate even when it is positioned at a steep angle. Conversely, heavier elements like Zr and Ta tend to travel in straighter trajectories, resulting in a lower flux arriving at the oblique substrate [23].

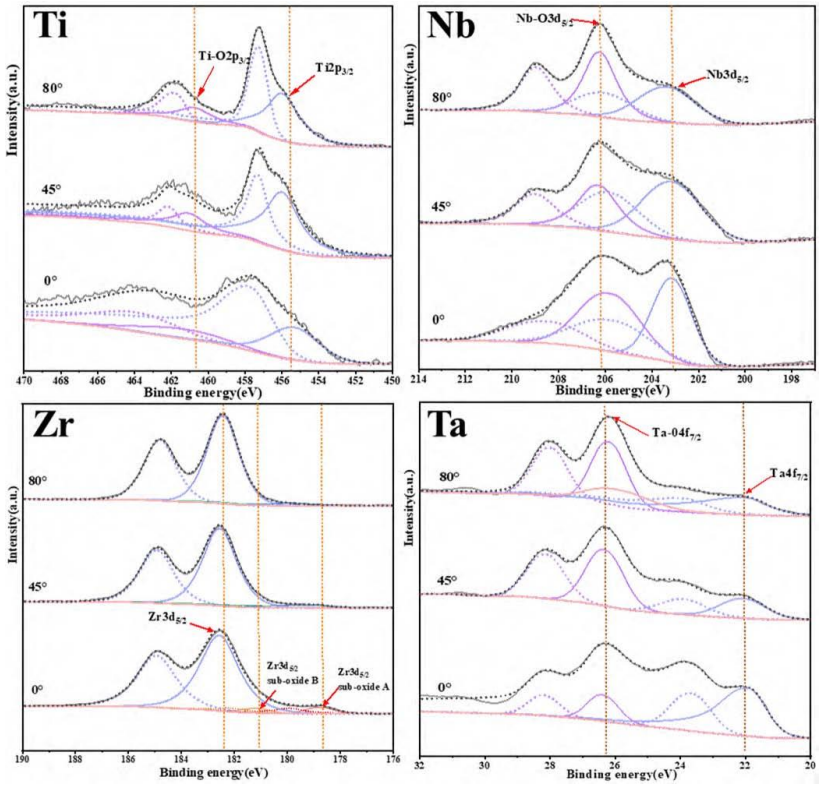

Figure 2 XPS spectra of Ti, Nb, Zr, and Ta for films deposited at different incident angles

XPS analysis provided deeper insight into the chemical states of the elements (Fig. 2). For the film deposited at 0°, the XPS spectra of Ti 2p, Zr 3d, Ta 4f, and Nb 3d were dominated by metallic peaks, with weak oxide peaks indicating a low degree of oxidation. As the incident angle increased to 45°, the metallic peaks attenuated while the oxide peaks grew in intensity. At 80°, the oxide peaks became dominant, signifying severe surface oxidation. Notably, the increase in oxidation state was more pronounced for Ti and Ta compared to Nb and Zr. This is consistent with the fact that the films deposited at higher incident angles possess a looser, more porous structure, which facilitates the adsorption of residual oxygen and water vapor from the vacuum chamber and promotes their reaction with the metal species. The increased path length for the depositing particles at higher incident angles, coupled with a constant partial pressure of background gases, creates a more oxidizing environment at the growing film surface [24].

3.2 Crystal Structure and Phase Constitution

The X-ray diffraction profiles for the Ti-Nb-Zr-Ta MEA coatings are illustrated in Fig. 3. All deposited films manifested a monophasic body-centered cubic crystalline structure, consistent with the phase constitution of conventionally cast Ti-Nb-Zr-Ta alloys [7]. This phase selection is governed by the alloy's average valence electron concentration (VEC ≈ 4.5) and atomic size mismatch (δ ≈ 9.4%), which favor the stabilization of the BCC lattice according to Hume-Rothery rules [25]. The diffraction peaks exhibited a clear trend of peak broadening, intensity reduction, and a shift toward lower 2θ angles as the incident angle increased. Peak broadening and attenuation signify diminished crystalline perfection and refined grain dimensions, attributable to the shadowing phenomenon restricting adatom surface mobility and impeding development of extensive, highly ordered crystalline domains [22]. The angular displacement toward lower diffraction angles indicates lattice parameter expansion, presumably arising from interstitial oxygen incorporation and solid solution formation with divergent unit cell dimensions [27].

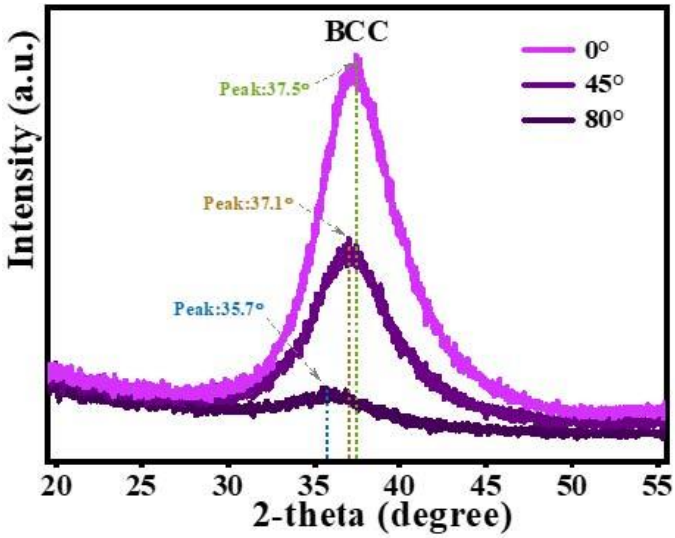

Figure 3 XRD patterns (phase constitution) of Ti-Nb-Zr-Ta medium-entropy alloy films deposited at different incident angles

3.3 Microstructure and Morphology Evolution

Cross-sectional SEM images (Fig. 4a-c) revealed the characteristic columnar microstructure of the films. The film thickness decreased dramatically with increasing incident angle, from approximately 2250 nm at 0° to 1000 nm at 45° and 450 nm at 80°.

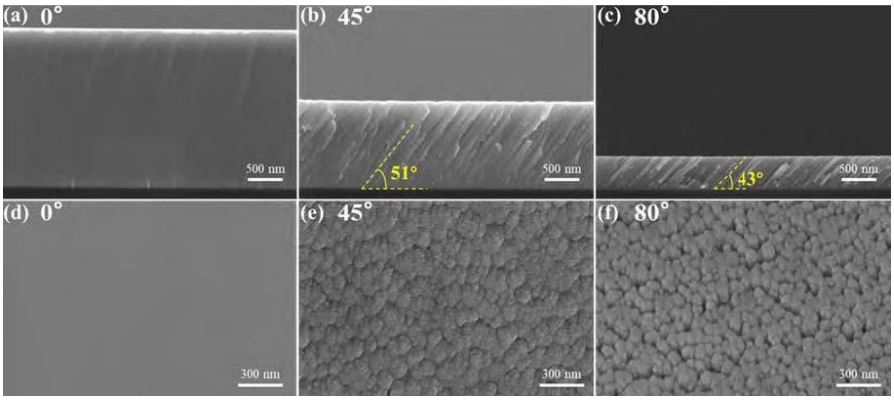

Figure 4 Morphology of Ti-Nb-Zr-Ta films deposited at different incident angles: cross-section (a–c); surface (d–f)

This thickness attenuation reflects diminished deposition kinetics, as the effective incident particle flux impinging upon the substrate surface decreases with increasing angular deviation from the target's central emission axis. The columnar grains exhibited a distinct tilting behavior; the angle between the columns and the substrate normal decreased from 90° (vertical) at 0° to 51° at 45° and 43° at 80°. Surface SEM images (Fig. 4d-f) corroborated this trend, showing that the film deposited at 0° had a smooth and dense surface, whereas the films deposited at 45° and 80° exhibited progressively rougher and more porous surface morphologies.AFM analysis (Fig. 5) quantified this trend, showing that the root-mean-square (RMS) surface roughness increased from 0.50 nm for the 0° film to 4.66 nm for the 45° film and 4.97 nm for the 80° film. This increase in roughness is a hallmark of the shadowing instability during oblique angle deposition. As adatoms arrive at the surface at a shallow angle, they are more likely to stick to the "windward" side of existing protrusions, leaving the "leeward" side in a shadow, devoid of new material. In the absence of sufficient thermal energy for surface diffusion to backfill these shadowed regions, a porous, columnar structure with high surface roughness naturally evolves [28].

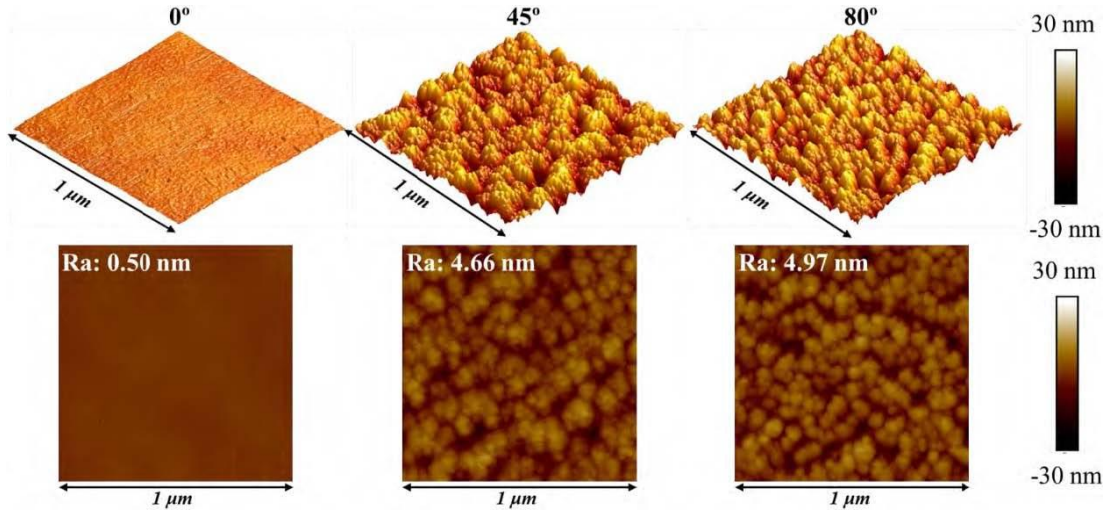

Figure 5 Surface topography and roughness of Ti-Nb-Zr-Ta films deposited at different incident angles

3.4 Optical Absorption and Photothermal Conversion

To investigate the absorption rate of Ti-Nb-Zr-Ta medium entropy alloy thin films in the 200–1200 nm optical wavelength range, tests were conducted using an ultraviolet-visible spectrophotometer (UV-Vis), and the results are shown in Figure 6. Ti-Nb-Zr-Ta medium entropy alloy coatings fabricated at varying deposition angles demonstrated appreciable optical absorption characteristics. This phenomenon originates from electronic state hybridization among the four constituent elements—Ti, Nb, Zr, and Ta—which elevates the density of states and enhances electron scattering probability, consequently amplifying the coating's photon capture efficiency [29].

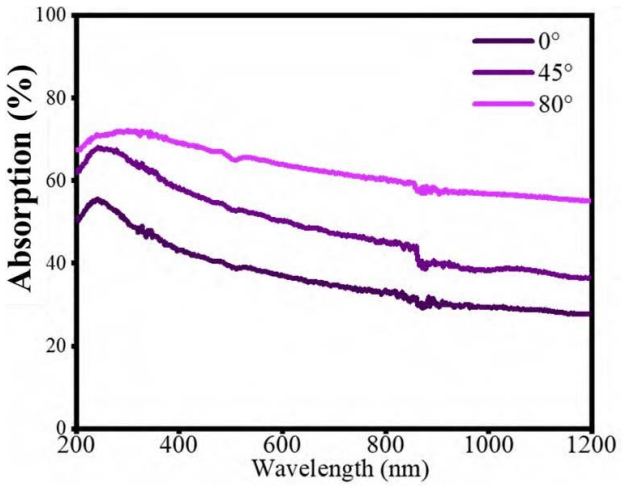

Figure 6 UV–Vis absorptance spectra of Ti-Nb-Zr-Ta films deposited at different incident angles

Furthermore, as shown in Figure 2, the chemical valence state results of the elements in the films indicate that as the incident angle for film deposition increases, the degree of oxidation of the film intensifies. Oxygen enters the lattice to form sub-oxides or oxygen vacancies, generating intraband states and narrowing the effective bandgap, thereby reducing the film's reflection and transmission of light and significantly enhancing the film's absorption of visible-near-infrared light [30]. Ultimately, elevated deposition angles correlated with enhanced optical absorption efficiency of the deposited coatings. As shown in Figures 4 and 5, the micro-morphology test results of Ti-Nb-Zr-Ta medium entropy alloy thin films show that as the incident angle for film deposition increases, the surface roughness of the Ti-Nb-Zr-Ta medium entropy alloy thin films increases, and the film structure becomes loose. After light enters the film surface, these rough structures form complex light traps [31], increasing the propagation path of light within the film and improving the film's absorption rate for light.

In this investigation, numerical simulations were executed via COMSOL Multiphysics 6.2 employing the finite element methodology. A planar two-dimensional representation derived from cross-sectional microstructural observations was adopted to minimize computational overhead and subjective bias. Two distinct geometric configurations—a planar smooth surface architecture and an inclined columnar morphology—were reconstructed based on scanning electron microscopy findings. After setting material parameters, periodic boundary conditions were set on the left and right boundaries, and ports were set on the upper and lower boundaries. After mesh generation, time-domain finite difference simulations were used to explore the electric field enhancement distribution of the models under 808 nm light irradiation wavelength, studying the plasmonic resonance phenomenon of the films. The results are shown in Figure 7. Smooth Ti-Nb-Zr-Ta medium entropy alloy thin films deposited at normal incidence exhibit a plasmonic resonance phenomenon, which is attributed to the hybridization of the four elements—Ti, Nb, Zr, and Ta—increasing the density of states. Meanwhile, compared to the smooth film at normal incidence, the plasmonic resonance of the loose film deposited at oblique incidence is stronger. As shown in Figure 4, the Ti-Nb-Zr-Ta medium entropy alloy thin films deposited at oblique incidence possess loose nanocolumnar crystals. This nanocolumnar crystal structure can excite longitudinal and transverse plasmonic resonances, producing strong near-field effects, efficiently converting incident light into heat or electronic excitation, thereby achieving broadband and efficient absorption of light [32]. Finally, increased oxidation leads to an increase in oxides such as TiOx and TaOx; the increased oxygen vacancies broaden the light absorption range and enhance near-infrared absorption as defect energy levels. Coupled with the loose columnar crystal structure acting as a "light trap" to enhance local electric fields and plasmonic resonance coupling, the photothermal conversion efficiency is further improved.

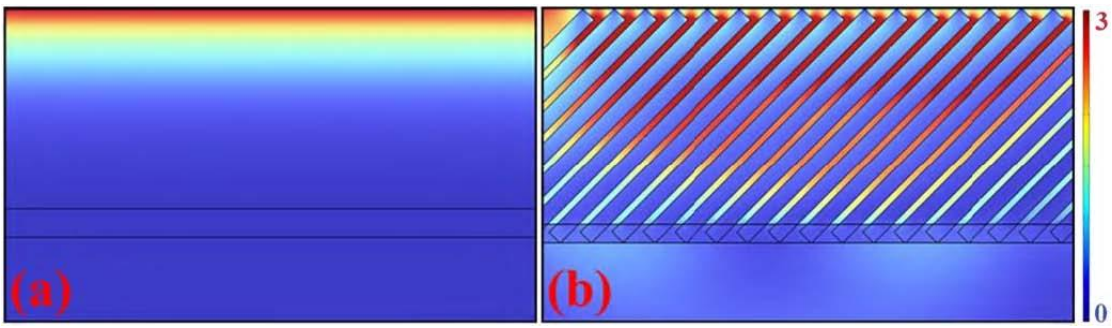

Figure 7 Simulated plasmonic resonance of Ti-Nb-Zr-Ta films: film deposited at 0° (a); film deposited at 80° (b)

Photothermal heating experiments were conducted using near-infrared lasers with power densities of 0.5 W/cm², 1 W/cm², and 2 W/cm², and a wavelength of 808 nm. The results are shown in Figure 8. Under continuous irradiation with near-infrared lasers at 0.5–2 W/cm², the temperature of the films rose rapidly, reaching a steady state after 3 minutes. With escalating laser irradiance, terminal film temperatures increased markedly. Even at modest power density (0.5 W/cm²), the normally deposited coating (0°) attained 42°C, confirming inherent photothermal transduction capacity of Ti-Nb-Zr-Ta medium entropy alloys. Comparative assessment across deposition geometries revealed a positive correlation between obliquity angle and photothermal response

magnitude under equivalent irradiance. Specifically, at 2 W/cm², the 80° oblique coating reached 110°C surface temperature, demonstrating substantial photothermal conversion efficiency in glancing-angle deposited Ti-Nb-Zr-Ta medium entropy alloy films.

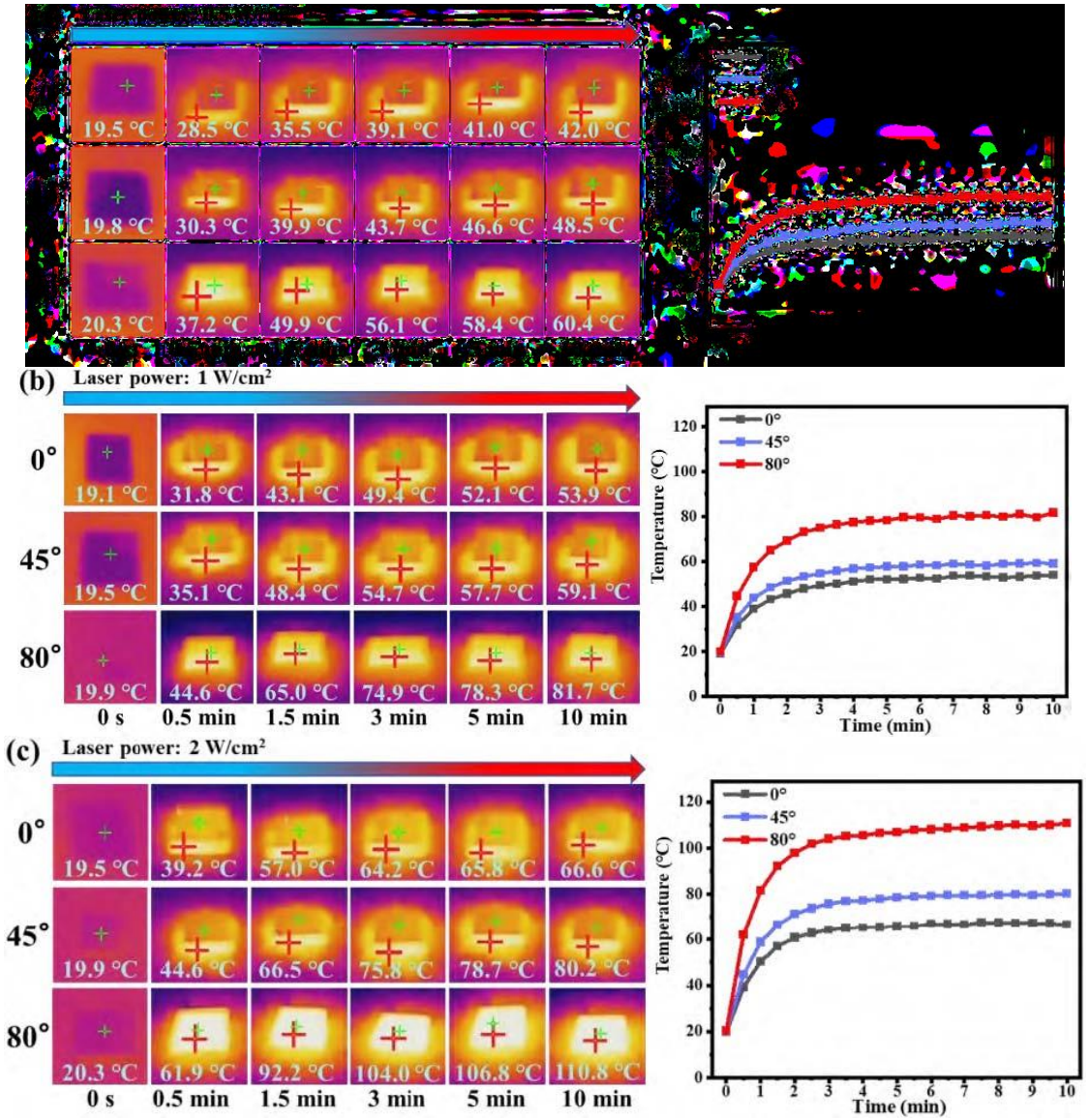

Figure 8 Photothermal heating profiles of Ti-Nb-Zr-Ta films surface under NIR irradiation at power densities of0.5 W/cm2 (a), 1 W/cm2 (b), 2 W/cm2 (c)

Films deposited at oblique incidence show intensified oxidation with increasing incident angle (Figure 2), which increases the film's optical absorption rate (Figure 6) and ultimately enhances the photothermal conversion capability of the Ti-Nb-Zr-Ta medium entropy alloy thin films (Figure 8). Simultaneously, films deposited at oblique incidence become structurally looser with increasing incident angle (Figures 4 and 5), possess more light traps, exhibit stronger plasmonic resonance phenomena (Figure 7), and improve the photothermal conversion capability of the Ti-Nb-Zr-Ta medium entropy alloy thin films. Finally, the poorer thermal conductivity of loose structures is advantageous for maintaining high temperatures in the films [33].

To characterize the photothermal stability of the Ti-Nb-Zr-Ta medium entropy alloy thin films, cyclic heating experiments were conducted. The experiment used a near-infrared laser with a power density of 2 W/cm² and a wavelength of 808 nm. The films underwent 10 cycles of laser irradiation and indoor air convection cooling.

The results are shown in Figure 9. Over 10 heating-cooling cycles, the difference in peak temperature for the films was less than 3°C, indicating that films deposited by all processes exhibited good photothermal conversion reversibility and stability. The repeatability of the heating-cooling waveforms for each cycle was high, with no significant drift or attenuation in peaks and valleys, suggesting that the films did not exhibit significant thermal fatigue or performance degradation after multiple thermal cycles. The Ti, Nb, Zr, and Ta elements selected in this study all possess high melting points and thermal stability. The Ti-Nb-Zr-Ta medium entropy alloy thin films composed of these elements also exhibit thermal stability, ensuring the reversibility and stability of the photothermal conversion capability.

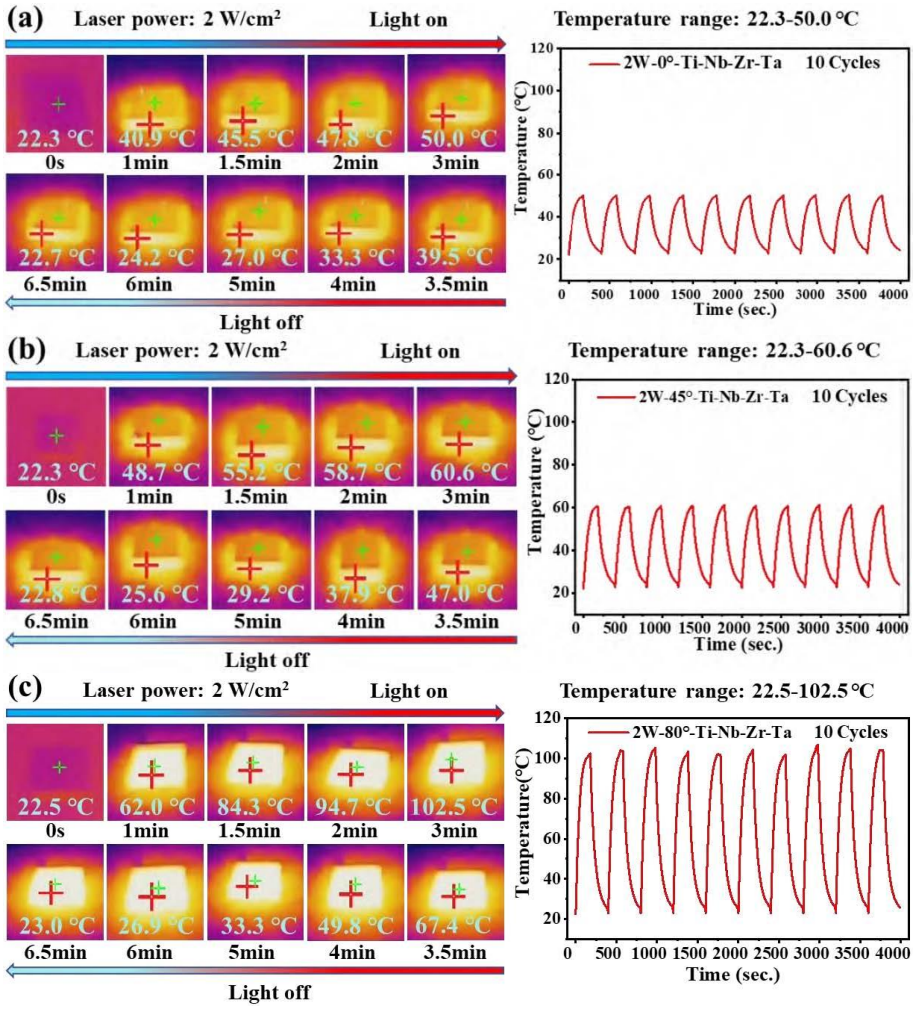

Figure 9 Photothermal heating–cooling cycles of Ti-Nb-Zr-Ta films deposited at0° (a), 45° (b), and 80° (c)

Comparing the magnitude of temperature change and the photothermal response speed, the Ti-Nb-Zr-Ta medium entropy alloy thin film deposited at an incident angle of 80° exhibited the highest photothermal temperature, reaching 100°C. Compared to the heating curves of films deposited at incident angles of 0° and 45°, its curve slope was larger, indicating a faster photothermal response speed. The film deposited at 80° exhibited higher oxidation and a looser structure, resulting in stronger optical absorption and plasmonic resonance, as well as lower thermal conductivity, leading to higher peak temperatures and faster photothermal response speeds.

In this study, the Ti-Nb-Zr-Ta medium entropy alloy thin film deposited at an incident angle of 80° experienced a temperature rise of 60°C after 3 minutes of irradiation with an 808 nm laser at 1 W/cm², with a heating rate reaching 20°C/min. Under the same experimental conditions, the surface temperature of an Au/SiO_2 nanocluster array increased by 30° C, with a heating rate of only 12° C/min [34]. Additionally, gold nanostructures may undergo morphological reconstruction under high-intensity lasers, causing absorption peak drift and weakening

photothermal effects. The Ti-Nb-Zr-Ta medium entropy alloy thin films deposited at oblique incidence maintained the highest temperature basically unchanged after multiple cycles of laser irradiation, indicating good repeatability and weather resistance of the film's photothermal performance.

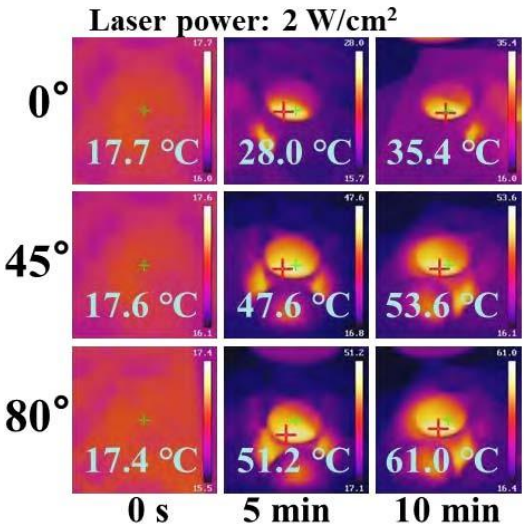

Figure 10 Photothermal properties of Ti-Nb-Zr-Ta films deposited at different incident angles under wet-state conditions

When the films are in service, they are surrounded by body fluids. To study the photothermal performance of the films in a wet state, samples were placed in a 24-well plate, and 800 µL of PBS solution was added. Continuous irradiation with an 808 nm laser was performed for 10 minutes, and the film surface temperature was recorded. The results are shown in Figure 10. The films also exhibited excellent photothermal performance in a simulated body fluid environment; the larger the incident angle, the higher the temperature of the deposited film. After 10 minutes of irradiation with a 2 W/cm² laser, the film deposited at an incident angle of 80° reached a surface temperature of 61°C, fully possessing the capability to kill bacteria.

The photothermal conversion efficiency ηof the films in the wet state was calculated using Formula (1) [35, 36]:

$$\eta = \frac{(C_s M_s + C_l M_l + C_f M_f)\Delta T}{IA\Delta t} \approx \frac{(C_s M_s + C_l M_l)}{IA}\frac{\Delta T}{\Delta t} \qquad (1)$$

ΔTrepresents the temperature rise of the sample (K); I, A, and Δtrepresent the laser power density, spot area, and irradiation time, respectively; Cs and Ms represent the specific heat capacity and mass of the 316L SS substrate; Cl and Ml represent the specific heat capacity and mass of PBS; Cf and Mf are the specific heat capacity and mass of the film. Since the film mass is much smaller than the substrate and culture medium mass, it was ignored in the calculation. Cs is 0.50 J/g·K, Ms is 0.97 g, Cl is 4.18 J/g·K, M is 0.80 g, Iis 2.00 W/cm², Ais 0.37 cm², and Δtis 10 min. This formulation exclusively accounts for internal energy accumulation within the system, neglecting thermal dissipation via convection, radiation, and conduction pathways; consequently, the derived photothermal conversion efficiency represents a conservative underestimate relative to actual performance. The experimental findings reveal: for normally deposited films (0°), conversion efficiency η equaled 30.7%; for moderately oblique deposition (45°), η reached 69.3%; for highly oblique deposition (80°), η attained 75.6%.

3.5 Photothermal Antibacterial and Biocompatibility Assessment

To evaluate the photothermal antimicrobial efficacy of the deposited coatings, *Escherichia coli* (ATCC 25922) was selected as a representative Gram-negative pathogen. Sterilized 316L stainless steel substrates—both uncoated and coated with Ti-Nb-Zr-Ta MEA films at varying deposition angles—were placed in individual wells. Each well received 800 µL bacterial inoculum at 3×10^8 CFU/mL. A bacterial suspension-only well served as negative control. All plates underwent 24 h incubation at 37°C with orbital agitation. Near-infrared irradiation

(808 nm, 2 W/cm²) was then administered for 10 min with the source positioned ~4 cm above the suspension surface. Non-irradiated counterparts served as dark controls. Post-treatment, 20 µL aliquots were spread-plated on nutrient agar, incubated at 37°C for 24 h, and enumerated for viable colony-forming units with photographic documentation. The results are shown in Figure 11.

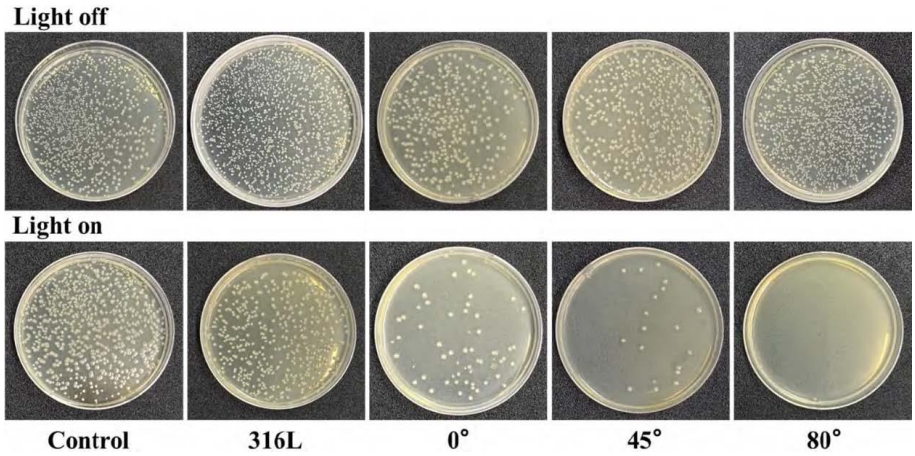

Figure 11 Photothermal antibacterial performance of Ti-Nb-Zr-Ta films deposited at different incident angles

Without laser irradiation (Light off), whether in the blank control (Control), 316L stainless steel, or films deposited at different incident angles, the agar plates were densely populated with colonies, and there was no significant difference between the groups. This indicates that the aforementioned samples basically exhibited no bactericidal capability without light. After laser irradiation (Light on), the Control group and the 316L group still had a high number of colonies; however, the three film samples exhibited photothermal antibacterial effects under laser irradiation. The film deposited at an incident angle of 80° showed the most significant bactericidal effect, with no colonies on the agar plate. As the incident angle during deposition decreased, the bactericidal capacity of the films decreased, yet it remained stronger than the Control group and the 316L group. The film deposited at 0° had an antibacterial rate of 87.66%; the film deposited at 45° had an antibacterial rate of 95.96%; the film deposited at 80° had an antibacterial rate of 99.99%.

Upon absorbing specific wavelengths of light, materials convert light energy into heat energy via non-radiative relaxation, forming localized high-temperature micro-regions at the material-bacteria interface. High temperatures can lead to structural damage to bacterial cell walls and membranes, imbalance in permeability with leakage of cellular contents, and induce irreversible denaturation of intracellular proteins and enzymes, metabolic collapse, and DNA damage, thereby causing bacterial inactivation [37]. After irradiation with laser light, the surface temperature of the Ti-Nb-Zr-Ta medium entropy alloy thin films rose rapidly, leading to the death of E. coli due to membrane protein denaturation, lipid phase transitions, and metabolic imbalances.

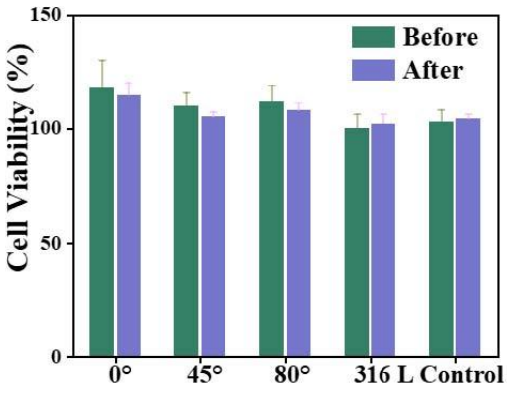

Figure 12 Fibroblast culture results on Ti-Nb-Zr-Ta film surfaces deposited at different incident angles before and after photothermal heating cycles

Studies on the composition, structure, and photothermal properties of films deposited at different incident angles show that the film deposited at 80° exhibits high oxidation, a loose porous surface, strong plasmonic resonance phenomena, the highest absorption rate for near-infrared light, and thus stronger photothermal conversion capability and photothermal stability. As the incident angle during deposition decreases, the degree of oxidation and the loose porous nature of the films both decrease. This reduces the film's absorption rate for near-infrared light and lowers the photothermal conversion capability, ultimately diminishing the photothermal antibacterial performance. However, due to the hybridization of the four elements—Ti, Nb, Zr, and Ta—which increases the density of states, the optical absorption rate of the films remains higher than that of the stainless steel substrate, thereby exhibiting superior photothermal antibacterial performance compared to the stainless steel substrate. Therefore, Ti-Nb-Zr-Ta medium entropy alloy thin films overall demonstrate photothermal antibacterial potential. Films deposited by the oblique incidence method further enhance this antibacterial performance.

To investigate the biocompatibility of the films, this experiment selected mouse epithelial fibroblasts (3T3) as model cells and used the Cell Counting Kit-8 (CCK-8) assay to evaluate cell viability. After 3 days of cell culture, the cells were diluted to a concentration of 3×10^5 cells/mL. Subsequently, 700 μL of the cell suspension was taken and co-cultured with the test samples under standard conditions (37°C, 5% CO_2) for 24 hours. Then, CCK-8 solution (with a volume ratio of CCK-8 to culture medium of 1:10) was added to each well, and the mixture was incubated for 2 hours under physiological conditions for color development. Finally, a multifunctional microplate reader (SpectraMax iD5, Molecular Devices, USA) was used to measure the optical density (OD) value at 450 nm to calculate the cell survival rate. The biocompatibility results of films deposited at different incident angles before and after photothermal heating cycles are shown in Figure 12.

Before the photothermal heating cycles, all films exhibited good cytocompatibility. The 0° group showed the highest viability (approximately 110%–120%), while the 45° and 80° groups remained in the range of approximately 105%–110%. After the photothermal heating cycles, due to the good thermal stability of the films, their cytocompatibility showed no significant difference compared to that before the cycles. The results indicate that the films have no obvious toxicity to fibroblasts. Ti-Nb-Zr-Ta medium entropy alloy thin films, composed of biologically inert Ti, Nb, Zr, and Ta elements, form a dense and stable oxide film on the surface, inhibiting metal ion release and ensuring the biological safety of the films and promoting cell proliferation.

4. Conclusion

This study successfully engineered Ti-Nb-Zr-Ta medium entropy alloy thin films with tailored photothermal and antibacterial properties via oblique-angle magnetron sputtering. By controlling the incident angle of deposition, we systematically modulated the film's composition, crystal structure, and, most importantly, its surface morphology. The key findings are as follows:

The crystal structure of the films was confirmed to be body-centered cubic (BCC). Increasing the incident angle from 0° to 80° resulted in a compositional shift towards higher Ti and Nb content and lower Zr and Ta content. The shadowing effect inherent to oblique deposition induced the formation of tilted, porous columnar grains and significantly increased surface roughness.

The photothermal performance was synergistically enhanced by three factors: (a) electronic hybridization increasing the density of states; (b) the "light trap" architecture of the porous columns causing multiple reflections; and (c) increased surface oxidation reducing reflectance. Consequently, the 80° film achieved a photothermal conversion efficiency of 75.6% and a temperature excursion of 110°C under NIR irradiation.

The intrinsic biocompatibility of the Ti-Nb-Zr-Ta system was preserved. Leveraging the light-trapping architecture and higher oxidation degree of the high-angle films, we achieved potent photothermal antibacterial activity (99.99% against E. coli) while maintaining cytocompatibility.

This work establishes oblique-angle magnetron sputtering as a versatile and scalable technique for fabricating architected MEA coatings. It provides a robust strategy for developing infection-resistant surfaces for biomedical implants, circumventing the need for antibiotic elution or the incorporation of potentially cytotoxic metal ions like silver or copper. The principles elucidated here—using geometry to control optical and thermal properties—may be broadly applicable to other bioinert alloy systems.

References

[1] HUSSEIN M A, KUMAR A M, AZEEM M A, et al. Development of Ti-Zr-Nb-Ta-Ag high entropy alloy for dental implants: In vitro corrosion behavior, antibacterial effect, and surface characteristics[J]. Materials Chemistry and Physics, 2021, 329: 130114.

[2] CHENG H H, MA H W, PAN L L, et al. Manufacturability and mechanical properties of Ti-35Nb-7Zr-5Ta porous titanium alloys produced by laser powder-bed fusion[J]. Additive Manufacturing, 2020, 86: 104190.

[3] EL-BASSYOUNI G T, MOUNEIR S M, EL-SHAMY A M, et al. Advances in surface modifications of titanium and its alloys: implications for biomedical and pharmaceutical applications[J]. Multiscale and Multidisciplinary Modeling, Experiments and Design, 2020, 8(5): 265.

[4] GUPTA S K, GUGULOTHU S B, IVANOV E, et al. Additive manufacturing of a low modulus biomedical Ti-Nb-Ta-Zr alloy by directed energy deposition[J]. Bioprinting, 2021, 41: e00349.

[5] GHODRATI H, GOODARZI A, GOLROKHIAN M, et al. A narrative review of recent developments in osseointegration and anti-corrosion of titanium dental implants with nano surface[J]. Bone Reports, 2020, 25: 101846.

[6] XIANG T, DU P, CAI Z, et al. Phase-tunable equiatomic and non-equiatomic Ti-Zr-Nb-Ta high-entropy alloys with ultrahigh strength for metallic biomaterials[J]. Journal of Materials Science & Technology, 2022, 117: 196-206.

[7] LI Z, LAI W, TONG X, et al. Design of TiZrNbTa multi-principal element alloys with outstanding mechanical properties and wear resistance[J]. Materials Science and Engineering: A, 2020, 845: 143203.

[8] MUSTAFI L, NGUYEN V T, LU S L, et al. Microstructure, tensile properties and deformation behaviour of a promising bio-applicable new Ti35Zr15Nb25Ta25 medium entropy alloy (MEA)[J]. Materials Science and Engineering: A, 2021, 824: 141805.

[9] GUO Y, WU J, XIE K, et al. Study of Bone Regeneration and Osteointegration Effect of a Novel Selective Laser-Melted Titanium-Tantalum-Niobium-Zirconium Alloy Scaffold[J]. ACS Biomaterials Science & Engineering, 2019, 5(12): 6463-6473.

[10] ACHACHE S, LAMRI S, ALHUSSEIN A, et al. Gum Metal thin films obtained by magnetron sputtering of a Ti-Nb-Zr-Ta target[J]. Materials Science and Engineering: A, 2016, 673: 492-502.

[11] BERNARD L, ARVIEUX C, BRUNSCHWEILER B, et al. Antibiotic Therapy for 6 or 12 Weeks for Prosthetic Joint Infection[J]. New England Journal of Medicine, 2021, 384(21): 1991-2001.

[12] LIU H Y, PRENTICE E L, WEBBER M A, et al. Mechanisms of antimicrobial resistance in biofilms[J]. npj Antimicrobials and Resistance, 2020, 2(1): 27.

[13] LEMIRE J A, HARRISON J J, TURNER R J, et al. Antimicrobial activity of metals: mechanisms, molecular targets and applications[J]. Nature Reviews Microbiology, 2013, 11(6): 371-384.

[14] TURNER R J. The good, the bad, and the ugly of metals as antimicrobials[J]. BioMetals, 2020, 37(3): 545-559.

[15] HU Y, LI S, DONG H, et al. Environment-Responsive Therapeutic Platforms for the Treatment of Implant Infection[J]. Advanced Healthcare Materials, 2021, 12(26): 2300985.

[16] XIN H, LIU Y, XIAO Y, et al. Design and Nanoengineering of Photoactive Antimicrobials for Bioapplications: from Fundamentals to Advanced Strategies[J]. Advanced Functional Materials, 2020, 34(38): 2402607.

[17] HE C Y, LI Y, ZHOU Z H, et al. High-Entropy Photothermal Materials[J]. Advanced Materials, 2020, 36(24): 2400920.

[18] NABAVI HAMEDANI S A, AMJAD-IRANAGH S, DEHGHANI K, et al. Photothermal high-entropy materials: A review[J]. Sustainable Materials and Technologies, 2021, 43: e01316.

[19] QIU Y, THOMAS S, GIBSON M A, et al. Corrosion of high entropy alloys[J]. npj Materials Degradation, 2017, 1(1): 15.

[20] CUI X, RUAN Q, ZHUO X, et al. Photothermal Nanomaterials: A Powerful Light-to-Heat Converter[J]. Chemical Reviews, 2020, 123(11): 6891-6952.

[21] ZHAO L, LIU Z, CHEN D, et al. Laser Synthesis and Microfabrication of Micro/Nanostructured Materials Toward Energy Conversion and Storage[J]. Nano-Micro Letters, 2021, 13(1): 49.
[22] BARRANCO A, BORRAS A, GONZALEZ-ELIPE A R, et al. Perspectives on oblique angle deposition of thin films: From fundamentals to devices[J]. Progress in Materials Science, 2016, 76: 59-153.
[23] XIA A, TOGNI A, HIRN S, et al. Angular-dependent deposition of MoNbTaVW HEA thin films by three different physical vapor deposition methods[J]. Surface and Coatings Technology, 2020, 385: 125356.
[24] BOUAOUINA B, MASTAILL C, BESNARD A, et al. Nanocolumnar TiN thin film growth by oblique angle sputter-deposition: Experiments vs. simulations[J]. Materials & Design, 2018, 160: 338-349.
[25] ALAM K, JANG W, JEONG G, et al. Design and Development of High-Entropy Alloys with a Tailored Composition and Phase Structure Based on Thermodynamic Parameters and Film Thickness Using a Novel Combinatorial Target[J]. ACS Omega, 2020, 8(31): 28333-28343.
[26] CHEN W, HILHORST A, BOKAS G, et al. A map of single-phase high-entropy alloys[J]. Nature Communications, 2021, 14(1): 2856.
[27] SEKKAT A, LIEDKE M O, NGUYEN V H, et al. Chemical deposition of Cu2O films with ultra-low resistivity: correlation with the defect landscape[J]. Nature Communications, 2022, 13(1): 5322.
[28] RAHMOUNI K, BENSALEM I, BENHAYA A, et al. Electrical resistivity, wettability, and structural properties of oriented columnar Mo thin films[J]. Thin Solid Films, 2020, 814: 140632.
[29] CHING W Y, SAN S, BRECKTL J, et al. Fundamental electronic structure and multiatomic bonding in 13 biocompatible high-entropy alloys[J]. npj Computational Materials, 2020, 6(1): 45.
[30] HOU X, ZHANG H, RAJU R, et al. Fast formation of thin TiOx layer on titanium surface enabling a broadband light capture and fast charge carrier transfer[J]. Journal of Power Sources, 2021, 580: 233281.
[31] DAS A, SINGH N K, SINGH L R, et al. Improved optical and electrical response by glancing angle synthesized Al2O3 nanorod array device[J]. Journal of Vacuum Science & Technology B, 2020, 42(2).
[32] JEN Y J, YANG K B, LIN P C, et al. Deposited ultra-thin titanium nitride nanorod array as a plasmonic near-perfect light absorber[J]. Scientific Reports, 2020, 10(1): 22269.
[33] AMAYA C, PRIAS-BARRAGAN J J, APERADOR W, et al. Thermal conductivity of yttria-stabilized zirconia thin films with a zigzag microstructure[J]. Journal of Applied Physics, 2017, 121(24).
[34] ZIESMER J, SONDN I, THERSLEFF T, et al. Highly Efficient Near-IR Photothermal Microneedles With Flame-Made Plasmonic Nanoaggregates For Reduced Intradermal Nanoparticle Deposition[J]. Advanced Materials Interfaces, 2022, 9(34): 2201540.
[35] REN D, CHEN M, WEI L, et al. Structure and photothermal performance of TaN films tailored by nitrogen flow rate and oblique angle sputtering for efficient antibacterial applications[J]. Surface and Coatings Technology, 2020: 132929.
[36] JIN H, LIN G, BAI L, et al. Photothermal conversion efficiency of nanofluids: an experimental and numerical study[J]. Solar Energy, 2016, 139: 278-289.
[37] CHEN X, LIN Z M, CHENG N, et al. Recent Advances In NIR-II Photothermal And Photodynamic Therapies For Drug-Resistant Wound Infections[J]. Materials Today Bio, 2021, 32: 101871.